

# Anomaly Detection via Mean Shift Density Enhancement

Pritam Kar<sup>1</sup>

Rahul Bordoloi<sup>2</sup>

Olaf Wolkenhauer<sup>2,3,4</sup>

Saptarshi Bej<sup>1</sup>

<sup>1</sup>School of Data Science, Indian Institute of Science Education and Research, India

<sup>2</sup>Institute of Computer Science, University of Rostock, Germany

<sup>3</sup>Leibniz-Institute for Food Systems Biology, Technical University of Munich, Germany

<sup>4</sup>Stellenbosch Institute of Advanced Studies (STIAS), South Africa

## Abstract

Unsupervised anomaly detection stands as an important problem in machine learning, with applications in financial fraud prevention, network security and medical diagnostics. Existing unsupervised anomaly detection algorithms rarely perform well across different anomaly types, often excelling only under specific structural assumptions. This lack of robustness also becomes particularly evident under noisy settings.

We propose *Mean Shift Density Enhancement* (MSDE), a fully unsupervised framework that detects anomalies through their *geometric response* to density-driven manifold evolution. MSDE is based on the principle that normal samples, being well supported by local density, remain stable under iterative density enhancement, whereas anomalous samples undergo large cumulative displacements as they are attracted toward nearby density modes.

To operationalize this idea, MSDE employs a weighted mean-shift procedure with adaptive, sample-specific density weights derived from a UMAP-based fuzzy neighborhood graph. Anomaly scores are defined by the total displacement accumulated across a small number of mean-shift iterations.

We evaluate MSDE on the ADBench benchmark, comprising forty six real-world tabular datasets, four realistic anomaly generation mechanisms, and six noise levels. Compared to 13 established unsupervised baselines, MSDE achieves consistently strong, balanced and robust performance for AUC-ROC, AUC-PR, and Precision@n, at several noise levels and on average over several types of anomalies. These results demonstrate that displacement-based scoring provides a robust alternative to the existing state-of-the-art for unsupervised anomaly detection.

## 1 Introduction

Anomaly detection is a fundamental problem in machine learning with applications in fraud detection, network intrusion monitoring, medical diagnostics, and several other fields. In many real-world settings, anomalies do not simply manifest as isolated outliers in Euclidean space; instead, they appear as subtle deviations from the underlying structure of a complex data manifold.

To better reflect real-world heterogeneity, ADBench organizes anomalies according to the scale and structure in which they occur. The benchmark distinguishes between anomalies that are isolated from the global distribution, those that deviate only within a local context, small abnormal groups that violate cluster-level assumptions, and samples that disrupt multivariate feature dependencies. A summary of this taxonomy is provided in Table 1.

Table 1: Overview of anomaly types used in the ADBench benchmark.

Anomaly Type	Description
Global anomalies	Samples that deviate significantly from the overall data distribution and are isolated in the feature space. These anomalies are typically far from dense regions and are often detectable by global distance- or density-based methods.
Local anomalies	Samples that appear normal with respect to the global distribution but are anomalous relative to their local neighborhood. These anomalies are embedded within dense regions yet exhibit subtle deviations from local structure, making them challenging for global detectors.
Cluster anomalies	Small or sparse clusters of samples that are internally coherent but differ from dominant clusters in the dataset. Such anomalies violate assumptions of cluster size or density and are often difficult to detect using point-wise outlier criteria alone.
Dependency anomalies	Samples that individually appear normal in marginal feature distributions but violate dependencies or correlations between features. These anomalies reflect structural inconsistencies rather than marginal extremeness and require detectors sensitive to multivariate relationships.

**Supervised anomaly detection.** In the fully supervised regime, anomaly detection reduces to binary classification, where labeled anomalies define discriminative decision boundaries (Table 2). Tree-based ensembles and gradient-boosted models such as LightGBM [Ke et al., 2017], XGBoost [Chen and Guestrin, 2016], and CatBoost [Prokhorenkova et al., 2018], as well as neural tabular architectures including ResNet-style models [He et al., 2016] and FT-Transformer [Gorishnyi et al., 2021], achieve strong performance when anomaly labels are abundant and representative. However, their reliance on labeled anomalies makes them vulnerable to label scarcity, selection bias, and shifts in anomaly semantics [Pang et al., 2021].

**Semi-supervised anomaly detection.** Semi-supervised methods exploit a limited number of anomaly labels to guide representation learning or score calibration (Table 2). Representative approaches include deviation-based learning (DevNet) [Pang et al., 2019], margin-based objectives (DeepSAD) [Ruff et al., 2020], and neighborhood-aware refinements such as PReNet and FEAWAD [Ren et al., 2019, Zhou et al., 2022]. Hybrid models like XGBOD [Zhao and Hryniwcki, 2018] integrate unsupervised signals into supervised learners. While semi-supervised anomaly detection (SSAD) [Yoo et al., 2025] improves robustness over fully supervised setups, performance remains sensitive to label noise and distributional drift

**Unsupervised anomaly detection.** In the absence of labeled anomalies, unsupervised anomaly detection dominates real-world deployments. Under the ADBench formulation [Han et al., 2022], given data  $X = x_{i=1}^n$  drawn from a mixture of mostly normal samples and a small fraction of anomalies, the goal is to assign anomaly scores  $s(x_i)$  based on structural assumptions about normality. As summarized in Table 2, these assumptions include geometric compactness, local density consistency, distributional regularity, and stability under random projections or reconstruction.

Table 2: Expanded taxonomy of anomaly detection paradigms, their modeling assumptions, and representative methods.

Paradigm / Family	Core Assumption / Signal	Scoring Mechanism	Representative Methods
Supervised AD	Labeled anomalies define decision boundary	Classification margin or posterior probability	LightGBM [Ke et al., 2017], XGBoost [Chen and Guestrin, 2016], CatBoost [Prokhorenkova et al., 2018]; tabular MLP, ResNet [He et al., 2016], FT-Transformer [Gorishniy et al., 2021]
Semi-supervised AD	Few anomaly labels refine representations or scores	Deviation, margin, or label-guided ranking	DevNet [Pang et al., 2019], DeepSAD [Ruff et al., 2020], PReNet [Ren et al., 2019], FEAWAD [Zhou et al., 2022], XGBOD [Zhao and Hryniwcki, 2018], SSAD [Yoo et al., 2025]
Projection-based	Normal data lie in low-dimensional subspace	Reconstruction error or projection residual	PCA [Shyu et al., 2003], OCSVM [Schölkopf et al., 2001]
Distance-based	Anomalies occur in sparse regions	$k$ -NN distance or rank statistics	KNN detector [Ramaswamy et al., 2000]
Local density-based	Anomalies deviate from neighbor-relative density	Density ratio or cluster-weighted score	LOF [Breunig et al., 2000], CBLOF [He et al., 2003], COF [Tang et al., 2002], SOD [Kriegel et al., 2009]
Distributional / statistical	Feature-wise or joint tail events	Histogram, copula, or ECDF tails	HBOS [Goldstein and Dengel, 2012], COPOD [Li et al., 2020], ECOD [Li et al., 2022]
Ensemble AD	Randomized partitions improve robustness	Average isolation depth or density	Isolation Forest [Liu et al., 2008], LODA [Pevný, 2016]
Deep unsupervised	Normal data form compact nonlinear manifold	Latent hypersphere or density estimate	DeepSVDD [Ruff et al., 2018], DAGMM [Zong et al., 2018]

**Projection and geometric methods.** Projection-based and large-margin methods assume that normal data occupy a compact subspace or region in feature space (Table 2). PCA-based detectors identify anomalies via unusually large reconstruction errors [Shyu et al., 2003], while one-class SVM (OCSVM) learns a high-margin boundary enclosing normal samples [Schölkopf et al., 2001, Pinon and Lartizien, 2025]. These approaches remain effective for low- to medium-dimensional tabular data but degrade under heterogeneous or highly nonlinear manifolds.

**Distance- and density-based methods.** Local modeling approaches formalize the intuition that anomalies occur in sparse or irregular neighborhoods (Table 2). KNN-based detectors score points by neighbor distances [Ramaswamy et al., 2000], while LOF [Breunig et al., 2000] and CBLOF [He et al., 2003] compare local density statistics. Extensions such as COF [Tang et al., 2002] and SOD [Kriegel et al., 2009] further account for connectivity and subspace relevance, enabling finer-grained local deviation detection.

**Distributional and ensemble detectors.** Distributional methods approximate anomaly likelihood through feature-wise or joint tail modeling (Table 2). HBOS [Goldstein and Dengel, 2012], COPOD [Li et al., 2020], and ECOD [Li et al., 2022] progressively trade modeling complexity for scalability and robustness. Ensemble approaches such as Isolation Forest [Liu et al., 2008] and LODA [Pevny, 2016] aggregate randomized partitions or projections, yielding strong empirical performance and scalability.

**Deep unsupervised models.** Deep anomaly detection models learn nonlinear latent manifolds that better capture complex normal patterns (Table 2). DeepSVDD [Ruff et al., 2018] enforces compactness in latent space, while DAGMM [Zong et al., 2018] combines reconstruction and density estimation. Despite their expressive power, these methods often require careful hyperparameter tuning and exhibit sensitivity to optimization and contamination.

**Our contribution.** Despite extensive methodological diversity, ADBench experiments reveals that no single unsupervised method produces stable/robust performance across datasets, anomaly types and noise levels [Han et al., 2022].

To address these limitations, we propose *Mean Shift Density Enhancement* (MSDE), a non-parametric anomaly detection framework that exploits local geometric structure through an adaptive mean-shift mechanism. MSDE is motivated by two key observations: (i) anomalies tend to lie in regions of low or unstable local density, and (ii) iterative shifting toward locally estimated density modes naturally exposes such irregularities.

Unlike classical mean-shift methods, MSDE constructs data-dependent weights using a fuzzy neighborhood graph derived from UMAP [McInnes et al., 2018], enabling adaptation to heterogeneous manifolds and arbitrary data distributions. MSDE first builds an adaptive neighborhood graph, then estimates multi-scale, sample-specific density weights, and finally performs a weighted mean-shift procedure. The cumulative movement of each point across iterations serves as its anomaly score: points embedded deeply within the manifold shift minimally, whereas anomalous points undergo large, directed movement toward density modes. Our contributions are as follows:

1. **A displacement-based principle for anomaly detection.** We introduce cumulative geometric shift as a novel anomaly signal, moving beyond static density or distance measures. This criterion provides a principled and interpretable mechanism for distinguishing normal and anomalous samples based on their stability under iterative density enhancement.

**2. A manifold-adaptive mean-shift framework.** We develop a weighted mean-shift procedure in which neighborhood influence is governed by empirical density estimates derived from a UMAP-based fuzzy neighborhood graph. This enables MSDE to adapt naturally to heterogeneous data manifolds without explicit parametric assumptions.

Through extensive evaluation on the ADBench benchmark, we demonstrate that MSDE achieves consistently strong performance across diverse anomaly types and noise levels, outperforming 13 established unsupervised baselines on an average over different noise levels and anomaly types, even with a default parameter setting. MSDE thus offers a principled, manifold-aware approach to anomaly detection.

## 2 Mean Shift Density Enhancement

We propose **Mean Shift Density Enhancement (MSDE)**, a non-parametric anomaly detection method that detects anomalies by estimating the intrinsic structure of the data manifold through *adaptive neighborhood weighting* (explained in sections 2.1 and 2.2) and *iterative shifting of data points* (explained in section 2.3). MSDE assigns anomaly scores by measuring the cumulative deviation or shift of each point from its locally estimated density mode across multiple shift iterations.

Our method consists of three components: (i) construction of an adaptive neighborhood graph, (ii) estimation of empirical sample weights via a UMAP-based fuzzy neighborhood graph, and (iii) a mean-shift procedure on the learned manifold.

### 2.1 Adaptive Neighborhood Graph Construction

Let  $X = \{x_i\}_{i=1}^N \subset \mathbb{R}^d$  be the dataset,  $x_i$  being the rows of the data matrix. MSDE builds a local neighborhood structure using an approximate  $k$ -nearest neighbor graph constructed via NN-Descent in the current feature space. For each point  $x_i$ , we obtain

$$\mathcal{N}_k(x_i) = \{x_{i_1}, \dots, x_{i_k}\}, \quad (1)$$

where  $\mathcal{N}_k(x_i)$  denotes the  $k$  nearest neighbors of  $x_i$  identified through Euclidean distance queries using the NN-Descent algorithm. This neighborhood graph is recomputed at every mean-shift iteration to ensure that locality is defined with respect to the current estimate of the data manifold. Next, MSDE assigns *sample-specific weights* that reflect local density and neighborhood reliability.

### 2.2 Estimation of Empirical Neighborhood Weights

To construct robust, locality-aware weights, we compute a *fuzzy neighborhood graph* using the UMAP framework. For each mini-batch of size  $B$ , we compute a fuzzy simplicial set

$$G = \text{UMAPGraph}(X_{\text{batch}}) \text{ (see section 3.1 of McInnes et al. [2018])}, \quad (2)$$

where  $G \in [0, 1]^{B \times B}$  contains pairwise membership strengths. Each entry  $g_{ij}$  represents the membership strength between points  $x_i$  and  $x_j$  for indices  $i, j \in \{1, \dots, B\}$ . These values lie in the interval  $[0, 1]$  because the UMAP graph construction defines edge weights through a normalized exponential kernel and subsequent fuzzy set union operations, both of which produce values bounded between 0 and 1. Thus,  $g_{ij}$  can be interpreted as the degree to which  $x_i$  and  $x_j$  belong to the same local manifold region.

**Binary-search radius estimation.** A key component of MSDE is a binary-search procedure that identifies a radius  $\varepsilon$  for which at least a proportion  $\alpha$  of the data points satisfy the required neighborhood-density condition.

$$\#\{x_j : d_G(x_i, x_j) < \varepsilon\} > T_{\text{nbd}}, \quad (3)$$

where  $d_G$  denotes distances in the similarity space derived from  $G$ , and  $T_{\text{nbd}}$  is a predefined neighborhood-density threshold. If no radius satisfies the original density and proportion constraints, the conditions are automatically relaxed and the search is repeated; if still unsuccessful, the maximum observed distance is used as a fallback radius.

**Averaged multi-radius weighting.** We evaluate neighborhood densities at a sequence of decreasing radii

$$\varepsilon_1 = \varepsilon, \varepsilon_2 = \varepsilon - \Delta, \dots, \varepsilon_m = \varepsilon - (m-1)\Delta, \quad (4)$$

and define the empirical weight for the  $i$ -th sample as

$$w_i = \frac{1}{m} \sum_{r=1}^m \#\{x_j : d_G(x_i, x_j) < \varepsilon_r\}. \quad (5)$$

This yields smooth, stable weights capturing intrinsic density across multiple neighborhood scales.

Here, the decrement  $\Delta$  is computed automatically based on the radius  $\varepsilon$  obtained from the binary-search step. In the implementation,  $\Delta$  is set as

$$\Delta = \frac{\varepsilon - 10^{-6}}{m}, \quad (6)$$

ensuring that the sequence of radii  $\{\varepsilon_r\}_{r=1}^m$  decreases uniformly from the initial estimate  $\varepsilon$  toward a small positive value. This produces a set of progressively stricter neighborhood scales, allowing the algorithm to average density estimates across multiple granularities and thereby obtain smoother and more stable empirical weights.

### 2.3 Mean Shift on the Learned Manifold

Given empirical weights  $\{w_j\}$  and local neighborhoods  $\mathcal{N}_k(x_i)$  obtained via approximate nearest neighbor search, MSDE performs a *weighted mean-shift update* on the learned manifold. At iteration  $t$ , we first compute a locally weighted neighborhood mean

$$\mu_i^{(t)} = \sum_{x_j \in \mathcal{N}_k(x_i)} \tilde{w}_j x_j, \quad \tilde{w}_j = \frac{w_j}{\sum_{x_\ell \in \mathcal{N}_k(x_i)} w_\ell}. \quad (7)$$

We then update the position of  $x_i$  along the direction from  $x_i^{(t)}$  to  $\mu_i^{(t)}$  with a normalized, magnitude-scaled step:

$$x_i^{(t+1)} = x_i^{(t)} + \eta \left\| x_i^{(t)} - \mu_i^{(t)} \right\| \frac{\mu_i^{(t)} - x_i^{(t)}}{\left\| \mu_i^{(t)} - x_i^{(t)} \right\| + \epsilon}, \quad (8)$$

where  $\eta$  is a learning rate and  $\epsilon$  is a small constant for numerical stability. The instantaneous movement magnitude at iteration  $t$  is defined as

$$\delta_i^{(t)} = \left\| x_i^{(t+1)} - x_i^{(t)} \right\|. \quad (9)$$

We accumulate the total distance traveled by each point across  $T$  iterations:

$$D_i = \sum_{t=1}^T \delta_i^{(t)}. \quad (10)$$

## 2.4 Anomaly Scoring

Intuitively, *normal samples* lie close to high-density regions of the manifold and remain relatively stable during the mean-shift iterations, resulting in small cumulative movement  $D_i$ . In contrast, *anomalies*, being far from dense regions, are pulled significantly toward the manifold and therefore experience larger movement.

We normalize and transform the cumulative movement into anomaly scores using a sigmoid function  $s_i = \sigma(\text{scale}(D_i))$ , where  $\text{scale}(\cdot)$  denotes a standardization step (e.g., z-score normalization) and  $\sigma$  is the logistic function. Higher scores correspond to more anomalous samples.

**Stopping criterion.** The mean-shift iterations are terminated using a simple convergence test. Let  $\delta_i^{(t)} = \|x_i^{(t)} - \mu_i^{(t)}\|$  denote the movement of point  $x_i$  at iteration  $t$ . We monitor the average movement

$$\bar{\delta}^{(t)} = \frac{1}{N} \sum_{i=1}^N \delta_i^{(t)}. \quad (11)$$

The algorithm stops either when a maximum number of iterations  $T$  is reached or when the average movement falls below a small threshold  $\tau$ ,  $\bar{\delta}^{(t)} < \tau$ , indicating that the points have stabilized around the underlying density structure.

Table 3: Main MSDE parameters with mathematical notation, code names, descriptions, and default values.

Notation	Code Name	Description	Default
$k$	<code>k</code>	Number of nearest neighbors used in each mean-shift update.	100
$T_{\text{nbd}}$	<code>nbd_sample_count_threshold</code>	Minimum number of neighbors required inside the estimated radius during weight computation. Controls density sensitivity.	70
$\eta$	<code>learning_rate</code>	Learning rate controlling the magnitude of each mean-shift update.	0.1
$T$	<code>max_iters_shift</code>	Maximum number of mean-shift iterations.	6
$\tau$	<code>shift_threshold</code>	Stopping threshold: algorithm halts early when average movement drops below $\tau$ .	0.003
$m$	<code>max_iters_weight_count</code>	Number of radii used when averaging density counts to compute empirical weights.	4
$\alpha$	<code>satisfiability_proportion</code>	Fraction of samples that must meet the density condition during binary-search estimation of $\varepsilon$ .	0.3

## 2.5 Computational Complexity

Let  $N$  denote the number of samples,  $d$  the feature dimension,  $k$  the number of nearest neighbors,  $T$  the maximum number of mean-shift iterations,  $m$  the number of radii used for multi-scale density

---

**Algorithm 1** Mean Shift Density Enhancement (MSDE)

---

**Require:** Dataset  $X = \{x_i\}_{i=1}^N \subset \mathbb{R}^d$ , number of neighbors  $k$ , learning rate  $\eta$ , maximum shift iterations  $T$ , shift stopping threshold  $\tau$ , neighborhood count threshold  $T_{\text{nbd}}$ , number of radius levels  $m$ , satisfiability proportion  $\alpha$

**Ensure:** Anomaly scores  $\{s_i\}_{i=1}^N$

1: **Step 1: Density-aware weight estimation**

2: Partition  $X$  into batches (or use full dataset if small)

3: **for** each batch  $X_b$  **do**

4:   Compute approximate  $k$ NN using NNDescent

5:   Construct UMAP fuzzy simplicial graph  $G_b$

6:   Represent each point by its fuzzy similarity vector  $g_i$

7:   Compute pairwise Euclidean distances between  $\{g_i\}$

8:   Build KD-Tree on  $\{g_i\}$

9:   Find radius  $\varepsilon$  via binary search such that  $\#\{g_j : \|g_i - g_j\| < \varepsilon\} > T_{\text{nbd}}$  holds for at least  $\alpha|X_b|$  points

10:   **for**  $r = 1$  to  $m$  **do**

11:      $\varepsilon_r \leftarrow \varepsilon - (r - 1)\Delta$  (see equation 6)

12:     Count neighbors within radius  $\varepsilon_r$

13:   **end for**

14:   Assign weight  $w_i \leftarrow \frac{1}{m} \sum_{r=1}^m \#\{g_j : \|g_i - g_j\| < \varepsilon_r\}$

15: **end for**

16: **Step 2: Weighted mean-shift with dynamic neighborhoods**

17: Initialize shifted points  $x_i^{(0)} \leftarrow x_i$

18: Initialize cumulative displacement  $D_i \leftarrow 0$

19: **for**  $t = 0$  to  $T - 1$  **do**

20:   Build approximate  $k$ NN graph on  $\{x_i^{(t)}\}$  using NNDescent

21:   **for** each point  $x_i^{(t)}$  **do**

22:     Compute weighted mean  $\mu_i^{(t)} \leftarrow \sum_{j \in \mathcal{N}_k(x_i^{(t)})} \frac{w_j}{\sum_{\ell \in \mathcal{N}_k(x_i^{(t)})} w_\ell} x_j^{(t)}$

23:     Compute displacement  $\delta_i^{(t)} \leftarrow \|x_i^{(t)} - \mu_i^{(t)}\|$

24:     Update point  $x_i^{(t+1)} \leftarrow x_i^{(t)} + \eta \delta_i^{(t)} \frac{\mu_i^{(t)} - x_i^{(t)}}{\|\mu_i^{(t)} - x_i^{(t)}\| + \epsilon}$

25:     Accumulate  $D_i \leftarrow D_i + \delta_i^{(t)}$

26:   **end for**

27:   **if**  $\frac{1}{N} \sum_i \delta_i^{(t)} < \tau$  **then**

28:     **break**

29:   **end if**

30: **end for**

31: **Step 3: Anomaly scoring**

32: **for** each  $x_i$  **do**

33:    $D_i \leftarrow \sum_{t=0}^{T-1} \delta_i^{(t)}$

34:    $s_i \leftarrow \sigma(\text{scale}(D_i))$

35: **end for**

---

estimation, and  $B$  the batch size used in the weight computation.

**Neighborhood construction.** During each mean-shift iteration, MSDE constructs a local neighborhood graph using approximate  $k$ -nearest neighbor search via NN-Descent. NN-Descent empirically scales close to linear time for fixed  $k$  and typically incurs  $\mathcal{O}(Nk)$  time per construction. Since the neighborhood graph is recomputed at every iteration to reflect the evolving manifold structure, the total cost over  $T$  iterations is  $\mathcal{O}(TNk)$ .

**Fuzzy neighborhood graph and weight estimation.** Empirical sample weights are computed prior to the mean-shift stage using a UMAP-based fuzzy neighborhood graph. The data are processed in mini-batches of size  $B$ . For each batch, approximate  $k$ NN search and fuzzy simplicial set construction incur  $\mathcal{O}(Bk)$  time. The subsequent multi-radius density estimation evaluates neighborhood counts at  $m$  progressively decreasing radii using KD-tree range queries in the similarity space, resulting in an additional  $\mathcal{O}(mBk)$  cost per batch. Aggregated across all batches, the total complexity of weight estimation is  $\mathcal{O}(mNk)$ .

**Mean-shift updates.** At each mean-shift iteration, a weighted neighborhood mean is computed for all  $N$  samples using their  $k$  nearest neighbors in the  $d$ -dimensional feature space. This results in a per-iteration cost of  $\mathcal{O}(Nkd)$ . Over  $T$  iterations, the total cost of the mean-shift updates is  $\mathcal{O}(TNkd)$ .

**Overall complexity.** Combining all components, the overall time complexity of the proposed MSDE implementation is

$$\mathcal{O}(TNkd + TNk + mNk).$$

For typical settings where  $d \gg 1$ , the dominant term is  $\mathcal{O}(TNkd)$ . In practice, MSDE uses small values of  $T$  and  $m$  (Table 3), making it scalable to large tabular datasets.

Figure 4 in Appendix A illustrates the geometric behavior induced by MSDE on a representative dataset. As the neighborhood size  $k$  increases, the mean-shift dynamics become smoother and more global, revealing stable manifold cores while amplifying the displacement of samples weakly supported by local density. Importantly, anomaly scoring in MSDE is not based on the final embedding, but on the cumulative displacement incurred during this density-driven evolution.

### 3 Experimental Setup

To rigorously evaluate the proposed Mean Shift Density Enhancement (MSDE) method, we adopt the experimental protocol of the *ADBench* benchmark [Han et al., 2022], which provides a large-scale, systematic comparison framework for anomaly detection algorithms. ADBench consists of forty six real-world tabular datasets spanning diverse application domains and anomaly characteristics, and evaluates 30 anomaly detection methods under supervised, semi-supervised, and unsupervised settings. Since MSDE is a fully unsupervised method, our comparison focuses exclusively on unsupervised baselines.

**Compared methods.** We compare MSDE against 13 representative unsupervised anomaly detection algorithms included in ADBench. These methods cover a broad spectrum of modeling assumptions, including distance-based detectors (KNN, LOF, COF), density-based methods (HBOS, COPOD, ECOD), clustering-based approaches (CBLOF, SOD), subspace and projection-based

techniques (PCA, OCSVM), ensemble methods (Isolation Forest, LODA), and deep probabilistic models (DAGMM). This diverse selection ensures a fair and comprehensive assessment across classical, ensemble-based, and deep unsupervised paradigms. All methods are evaluated in a strictly unsupervised setting, with no access to anomaly labels during training or scoring. Following the ADBench protocol, experiments are conducted across all datasets using four realistic synthetic anomaly generation modes (global, local, cluster and dependency) across 3 random seeds as detailed in Table 1.

**Noise injection and robustness evaluation.** In addition to varying anomaly types, we evaluate the robustness of all methods under different levels of feature noise, following the ADBench experimental design. Specifically, independent noise is injected into the data at six different noise ratios, ranging from noise-free settings to progressively higher noise levels. This perturbation simulates measurement errors, sensor noise, and irrelevant feature corruption commonly encountered in real-world tabular datasets. Performance is reported separately for each noise level to assess the stability and degradation behavior of anomaly detectors under increasing noise.

**Performance measures.** We report results using three complementary evaluation metrics: Area Under the Receiver Operating Characteristic curve (AUC-ROC), Area Under the Precision–Recall curve (AUC-PR), and Precision@n.

**AUC-ROC** measures the ability of a detector to rank anomalous samples ahead of normal ones across all possible decision thresholds, making it a standard metric for anomaly detection benchmarks. However, AUC-ROC can be overly optimistic in highly imbalanced settings, which are common in anomaly detection.

**AUC-PR** focuses on the precision–recall trade-off and is particularly sensitive to class imbalance. It emphasizes the correctness of anomaly rankings when anomalies constitute a small fraction of the data, thereby providing a more informative assessment of detector performance in practical scenarios.

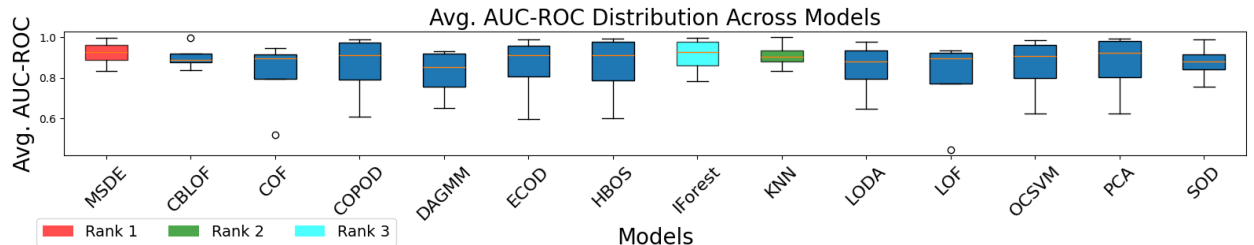
**Precision@n** evaluates the fraction of true anomalies among the top- $n$  highest-scoring samples, where  $n$  equals the number of ground-truth anomalies in each dataset. Unlike threshold-independent metrics, Precision@n directly measures the quality of the top-ranked detections and reflects real-world use cases in which only a limited number of flagged instances can be manually inspected. Although Precision@n is not originally reported in ADBench, we include it as a complementary metric to better assess extreme-tail anomaly ranking performance.

**Implementation details.** All baseline methods are implemented using the official ADBench codebase with default hyperparameters, ensuring consistency with prior evaluations. MSDE is implemented without dataset-specific tuning. Unless stated otherwise, all experiments are conducted using the default MSDE parameters described in Table 3. This design choice emphasizes robustness and reproducibility across heterogeneous datasets, anomaly types and noise settings.

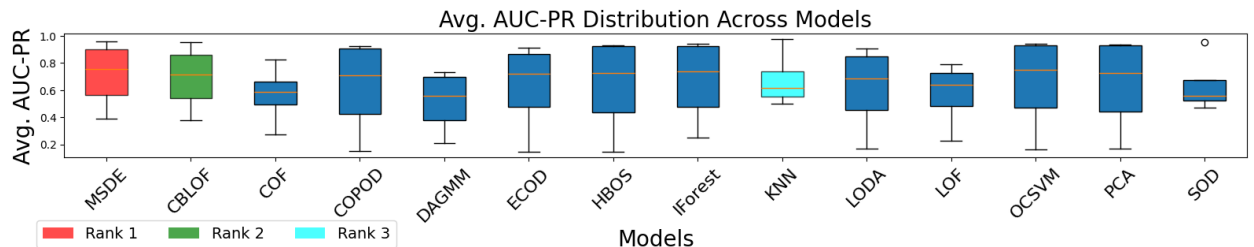
Our experimental setup enables a fair, comprehensive, and reproducible comparison of MSDE against established unsupervised anomaly detection methods under realistic and challenging benchmark conditions.

## 4 Results

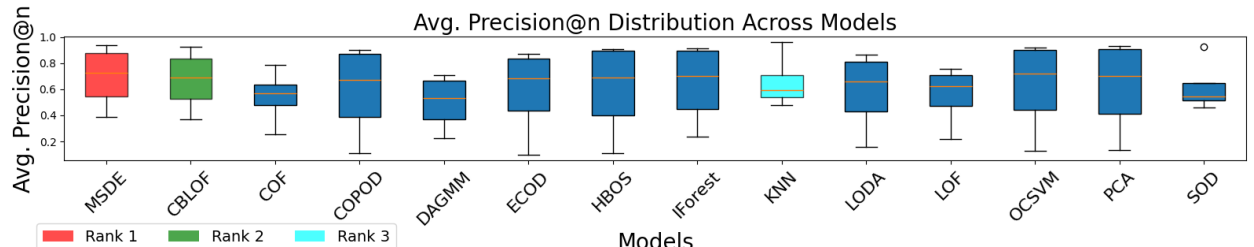
We evaluate the proposed Mean Shift Density Enhancement (MSDE) method under the unsupervised ADBench protocol, considering both noise-free and noisy settings. Performance is assessed



(a) AUC-ROC



(b) AUC-PR



(c) Precision@N

Figure 1: Performance comparison of anomaly detection methods under no noise across evaluation metrics. Under the zero noise setting, MSDE outperforms other models on average over different anomaly types.

using three complementary metrics: AUC-ROC, AUC-PR, and Precision@n. Results are averaged over all datasets and three random seeds, ensuring robust comparisons.

**Performance across synthetic anomaly generation modes.** To assess robustness across different anomaly mechanisms, we analyze MSDE’s performance separately under the four synthetic anomaly generation modes used in ADBench: dependency, cluster, global, and local anomalies. Table 7 in Appendix A provides the full per-method results in zero noise settings.

For *global anomalies*, nearly all methods perform well due to the clear separation between anomalous and normal samples. MSDE ranks second across AUC-ROC, AUC-PR, and Precision@n, with performance (0.998/0.958/0.935) closely trailing KNN, which achieves the highest scores in this mode.

In the *local anomaly* setting, MSDE ranks fourth in AUC-ROC and third in both AUC-PR and Precision@n. Here, MSDE is outperformed primarily by LOF and KNN, which are explicitly designed to exploit local density ratios and nearest-neighbor distances.

For *cluster anomalies*, projection- and variance-based methods such as PCA, HBOS, OCSVM, and COPOD outperform MSDE by exploiting strong inter-cluster separability and global variance structure. These methods benefit from the presence of compact, well-separated anomalous clusters that violate global distributional assumptions. Although quite a strong performer in other modes, the performance of KNN is notably weak in this mode.

The most challenging setting is *dependency anomalies*, where MSDE ranks between 5 and 6 across metrics. In this mode, MSDE is outperformed by methods such as COF, LOF, and KNN. Dependency anomalies violate feature correlations rather than marginal distributions, favoring detectors that encode relational structure more directly.

While individual baselines excel at specific anomaly mechanisms, MSDE is the only method that consistently maintains stable performance across all four synthetic modes. MSDE avoids catastrophic performance degradation in any single mode and offers a stable, general-purpose solution for heterogeneous anomaly detection scenarios. Aggregating performance across all four synthetic modes (Table 4), MSDE achieves the highest average AUC-ROC, AUC-PR, and Precision@n among all compared methods in the zero noise setting. Thus, MSDE offers balanced and consistently strong performance across diverse anomaly types.

**Performance under noise-free conditions and Robustness to increasing noise levels** In Table 5 we provide the ranks of all the compared algorithms across six different noise levels, giving insight into robustness under data corruption. For full per-method results under progressively increasing feature noise levels, see Table 6 in Appendix A. (0.00, 0.01, 0.05, 0.10, 0.25, 0.50). Results are averaged over the four different synthetic modes. As expected, all methods exhibit performance degradation as noise levels increase. However, MSDE exhibits a comparatively gradual and stable decline.

At nil/low to moderate noise levels (noise ratios 0.00–0.10), MSDE consistently achieves either the best or second-best performance across all three metrics. Notably, MSDE maintains AUC-ROC values above 0.92 up to a noise level of 0.10, indicating strong resilience to mild perturbations.

At higher noise levels (0.25 and 0.50), performance differences between methods narrow. In this regime, some baselines such as KNN and CBLOF occasionally attain higher AUC-PR or Precision@n scores. Nevertheless, MSDE remains competitive across all metrics and avoids the sharp performance collapse observed in reconstruction-based models, such as DAGMM, and purely local density estimators, such as LOF and COF.

Table 4: Average performance of anomaly detection methods across all four synthetic anomaly generation modes under zero noise setting.

Method	Avg AUC-ROC $\uparrow$	Avg AUC-PR $\uparrow$	Avg Precision@n $\uparrow$
MSDE	<b>0.922</b>	<b>0.714</b>	<b>0.694</b>
KNN	0.910	0.676	0.655
IForest	0.908	0.667	0.638
CBLOF	0.904	0.689	0.667
SOD	0.878	0.637	0.617
PCA	0.865	0.641	0.616
OCSVM	0.856	0.650	0.621
HBOS	0.853	0.632	0.600
COPOD	0.855	0.624	0.588
ECOD	0.852	0.625	0.585
LODA	0.847	0.612	0.583
COF	0.815	0.568	0.545
LOF	0.794	0.574	0.555
DAGMM	0.822	0.516	0.499

## 5 Discussion

**Effectiveness and Novelty of the MSDE Approach for Anomaly Detection.** The experimental results indicate that MSDE performs consistently well across all four synthetic anomaly generation modes and remains competitive across evaluation metrics and noise regimes. In particular, MSDE achieves high average performance across dependency, cluster, global, and local anomaly settings, and maintains strong performance under noise levels up to 0.1 (Table 5). Additionally, we performed a small scalability analysis of MSDE on the Credit Fraud Detection dataset [Le Borgne et al., 2022] ( $N = 284,807$ ) and found that MSDE is an order of magnitude faster than computationally intensive methods, such as KNN, DAGMM, SOD, and OCSVM, while maintaining its competitiveness in terms of AUC-ROC. Full details can be found in Appendix B.

MSDE scores anomalies based on cumulative geometric displacement induced by weighted mean-shift iterations rather than static distance or reconstruction error. Normal samples converge rapidly to nearby density modes and exhibit small cumulative movement, whereas anomalous samples undergo larger shifts before stabilization. This displacement-based scoring is a novel approach in the domain of unsupervised anomaly detection.

Figure 2 provides an intuitive interpretation of MSDE anomaly scores on image data. Digits that are visually ambiguous, distorted, or atypically written undergo significantly larger cumulative shifts, whereas clean and canonical digit instances remain stable. This behavior aligns with the core hypothesis of MSDE: normal samples are supported by strong local density and therefore resist displacement, while anomalous samples exhibit pronounced geometric instability.

**Limitations.** Despite its strengths, MSDE has several limitations. First, the method relies on nearest-neighbor graph construction and repeated mean-shift updates, which introduce computational overhead compared to simple histogram- or projection-based detectors. Although the use of approximate kNN search and a small number of shift iterations keeps the method practical for medium- to large-scale tabular datasets, further optimization would be required for extremely large or streaming data scenarios.

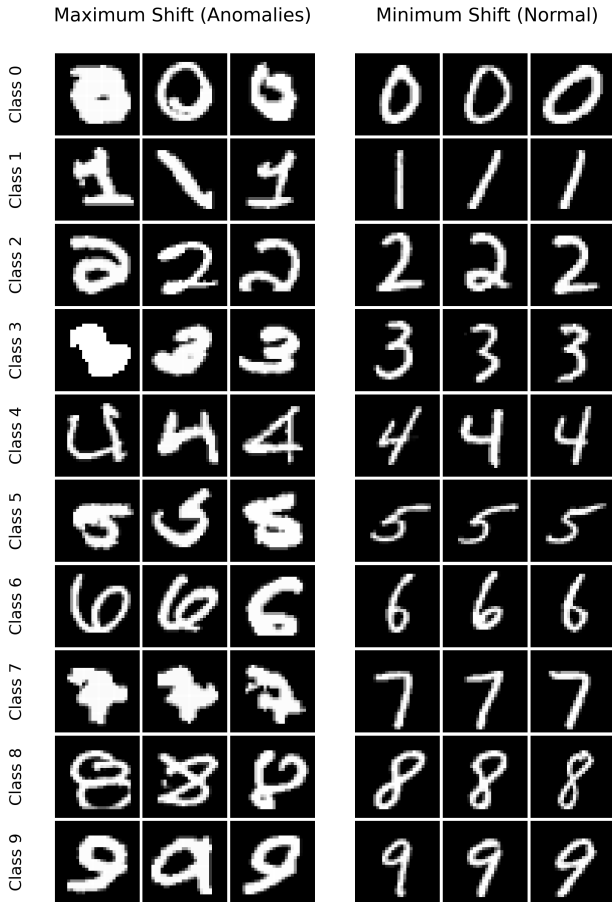


Figure 2: Qualitative illustration of MSDE anomaly detection on the MNIST dataset. **Left:** samples with the largest cumulative MSDE displacement (high anomaly scores). **Right:** samples with the smallest displacement (low anomaly scores). Across all digit classes, high-shift samples correspond to poorly written, ambiguous, or structurally irregular digits, while low-shift samples represent clean, prototypical instances. This demonstrates that MSDE captures semantic irregularity through geometric instability, despite operating in a fully unsupervised manner.

Table 5: Comma-separated ranks of anomaly detection methods across noise levels (0.00, 0.01, 0.05, 0.10, 0.25, 0.50) averaged over the four different synthetic modes. Lower rank indicates better performance.

Method	AUC-ROC Ranks	AUC-PR Ranks	Precision@n Ranks
MSDE	1, 1, 1, 2, 2, 6	1, 1, 1, 1, 2, 5	1, 1, 1, 1, 2, 5
CBLOF	4, 4, 4, 4, 4, 5	2, 2, 3, 3, 3, 2	2, 2, 3, 3, 3, 2
COF	13, 13, 12, 12, 13, 13	13, 13, 13, 13, 13, 13	13, 13, 13, 13, 13, 13
COPOD	8, 8, 7, 7, 8, 9	10, 10, 10, 9, 8, 8	9, 9, 9, 9, 9, 8
DAGMM	12, 12, 13, 14, 14, 14	14, 14, 14, 14, 14, 14	14, 14, 14, 14, 14, 14
ECOD	10, 10, 10, 9, 9, 8	9, 9, 9, 8, 7, 9	10, 10, 10, 10, 8, 9
HBOS	9, 9, 8, 8, 6, 4	8, 8, 8, 7, 6, 4	8, 8, 8, 7, 6, 4
IForest	3, 3, 3, 3, 3, 2	4, 4, 4, 4, 4, 6	4, 4, 4, 4, 4, 6
KNN	2, 2, 2, 1, 1, 1	3, 3, 2, 2, 1, 1	3, 3, 2, 2, 1, 1
LODA	11, 11, 11, 11, 10, 10	11, 11, 11, 11, 11, 12	11, 11, 11, 11, 11, 12
LOF	14, 14, 14, 13, 12, 12	12, 12, 12, 12, 12, 11	12, 12, 12, 12, 12, 11
OCSVM	7, 7, 9, 10, 11, 11	5, 5, 5, 6, 9, 10	5, 5, 5, 6, 10, 10
PCA	6, 6, 6, 6, 5, 3	6, 6, 6, 5, 5, 3	7, 7, 6, 5, 5, 3
SOD	5, 5, 5, 5, 7, 7	7, 7, 7, 10, 8, 8	6, 6, 7, 8, 7, 7

Second, MSDE assumes that meaningful local neighborhood structure exists in the feature space. In datasets where features are weakly informative or dominated by noise, the constructed manifold may be unreliable, limiting the effectiveness of density enhancement. We also observed that for very high noise levels (0.25 and 0.5) performance of MSDE degrades compared to lower noise levels (for further details see Table 6 in Appendix A). This limitation is shared by many geometry-based anomaly detection methods.

**Beyond anomaly detection: broader applications of density enhancement.** Beyond anomaly detection, MSDE introduces a general paradigm for *density-driven geometric evolution* of data that can be exploited in a variety of downstream tasks. The trajectories traced by samples during the mean-shift process encode rich structural information about the data manifold, rather than serving merely as an intermediate step for anomaly scoring.

The paths followed by points as they move toward local density modes can be interpreted as flow lines on the manifold, revealing shared local structure, boundary regions, and transitional states. Such trajectory-level information may be used for clustering directly in high-dimensional feature space, without relying on explicit dimensionality reduction.

The direction and magnitude of shifts in feature space further provide a principled basis for assessing feature relevance: dimensions that consistently drive large displacements may correspond to unstable or discriminative features, while stable coordinates remain largely unchanged. In Appendix A Figure 5, we visualize the mean absolute per-feature shift induced by MSDE on the MNIST dataset, aggregated class-wise. The resulting heatmaps reveal that MSDE concentrates displacement on semantically informative stroke regions rather than background pixels, further supporting the interpretation of MSDE as a structure-aware density enhancement process. In addition, the iterative movement toward dense regions implicitly suppresses noise, yielding a density-regularized representation that can benefit downstream tasks such as clustering or classification.

MSDE suggests a structure-aware data transformation framework in which iterative density

enhancement reveals latent geometric organization without altering the ambient feature space, opening avenues for integration with representation learning and graph-based models.

## 6 Conclusion

In this work, we introduced Mean Shift Density Enhancement, a non-parametric, fully unsupervised anomaly detection method that employs adaptive neighborhood modeling and iterative geometric refinement. Extensive evaluation on the ADBench benchmark demonstrates that MSDE achieves competitive or superior performance compared to established unsupervised baselines across multiple anomaly types, evaluation metrics, and noise levels. By framing anomaly detection as a density-driven dynamic process on the data manifold, MSDE provides both strong empirical performance and an interpretable geometric intuition. These properties make MSDE a promising and versatile tool for unsupervised anomaly detection, motivating further exploration of density enhancement techniques in broader machine learning applications.

## References

Markus M. Breunig, Hans-Peter Kriegel, Raymond T. Ng, and Jörg Sander. LOF: Identifying density-based local outliers. In *Proceedings of the ACM SIGMOD International Conference on Management of Data*, pages 93–104, 2000.

Tianqi Chen and Carlos Guestrin. Xgboost: A scalable tree boosting system. In *Proceedings of the ACM SIGKDD International Conference on Knowledge Discovery and Data Mining*, pages 785–794, 2016.

Markus Goldstein and Andreas Dengel. Histogram-based outlier score (HBOS). In *KI 2012: Poster and Demo Track*, 2012.

Yury Gorishniy, Ivan Rubachev, Valentin Khrulkov, and Artem Babenko. Revisiting deep learning models for tabular data. In *Advances in Neural Information Processing Systems (NeurIPS)*, 2021.

Songqiao Han, Xiyang Hu, Hailiang Huang, Minqi Jiang, and Yue Zhao. Adbench: Anomaly detection benchmark. In *Advances in Neural Information Processing Systems (NeurIPS), Datasets and Benchmarks Track*, 2022.

Kaiming He, Xiangyu Zhang, Shaoqing Ren, and Jian Sun. Deep residual learning for image recognition. In *Proceedings of the IEEE Conference on Computer Vision and Pattern Recognition (CVPR)*, pages 770–778, 2016.

Zengyou He, Xiaofei Xu, and Shengchun Deng. Discovering cluster-based local outliers. In *Proceedings of the 2003 International Conference on Data Mining*, 2003.

Guolin Ke, Qi Meng, Thomas Finley, Taifeng Wang, Wei Chen, Weidong Ma, Tie-Yan Ye, and Qi Liu. Lightgbm: A highly efficient gradient boosting decision tree. In *Advances in Neural Information Processing Systems (NeurIPS)*, 2017.

Hans-Peter Kriegel, Peer Kröger, Erich Schubert, and Arthur Zimek. Outlier detection in axis-parallel subspaces of high dimensional data. In *Pacific-Asia Conference on Knowledge Discovery and Data Mining (PAKDD)*, pages 831–838, 2009.

Yann-Aël Le Borgne, Wissam Siblini, Bertrand Lebichot, and Gianluca Bontempi. *Reproducible Machine Learning for Credit Card Fraud Detection - Practical Handbook*. Université Libre de Bruxelles, Belgium, 2022. URL <https://github.com/Fraud-Detection-Handbook/fraud-detection-handbook>.

Zheng Li, Yue Zhao, Mahsa Salehi, Ryan Li, Cyrus Shahabi, Vipin Kumar, and J. Zico Liu. COPOD: Copula-based outlier detection. In *IEEE International Conference on Data Mining (ICDM)*, 2020.

Zheng Li, Yue Zhao, Nicola Botta, Cătălin Ionescu, Xiyang Hu, and J. Zico Liu. ECOD: Unsupervised outlier detection using empirical cumulative distribution functions. *ACM Transactions on Knowledge Discovery from Data*, 2022.

Fei Tony Liu, Kai Ming Ting, and Zhi-Hua Zhou. Isolation forest. In *IEEE International Conference on Data Mining (ICDM)*, pages 413–422, 2008.

Leland McInnes, John Healy, and James Melville. Umap: Uniform manifold approximation and projection for dimension reduction. *arXiv preprint arXiv:1802.03426*, 2018.

Guansong Pang, Chunhua Shen, and Anton van den Hengel. Deep anomaly detection with deviation networks. In *Proceedings of the 25th ACM SIGKDD international conference on knowledge discovery & data mining*, pages 353–362, 2019.

Guansong Pang, Chunhua Shen, Longbing Cao, and Anton van den Hengel. Deep learning for anomaly detection: A review. *ACM Computing Surveys*, 54(2):1–38, 2021.

Tomáš Pevný. LODA: Lightweight on-line detector of anomalies. *Machine Learning*, 102(2):275–304, 2016.

Nicolas Pinon and Carole Lartizien. Ocsvm-guided representation learning for unsupervised anomaly detection, 2025. URL <https://arxiv.org/abs/2507.21164>.

Liudmila Prokhorenkova, Gleb Gusev, Andrey Vorobev, Anna Veronika Dorogush, and Dmitry Gulin. Catboost: Unbiased boosting with categorical features. *Advances in Neural Information Processing Systems (NeurIPS)*, 2018.

S. Ramaswamy, R. Rastogi, and K. Shim. Efficient algorithms for mining outliers from large data sets. In *Proceedings of the ACM SIGMOD International Conference on Management of Data*, pages 427–438, 2000.

Dongwei Ren, Wangmeng Zuo, Qinghua Hu, Pengfei Zhu, and Deyu Meng. Progressive image deraining networks: A better and simpler baseline. In *IEEE Conference on Computer Vision and Pattern Recognition*, 2019.

Lukas Ruff, Rêmi Vandermeulen, Nico Görnitz, Lucas Deecke, Shoaib Siddiqui, Alexander Binder, Klaus-Robert Müller, and Marius Kloft. Deep one-class classification. In *Proceedings of the 35th International Conference on Machine Learning (ICML)*, 2018.

Lukas Ruff, Robert A. Vandermeulen, Nico Görnitz, Alexander Binder, Emmanuel Müller, Klaus-Robert Müller, and Marius Kloft. Deep semi-supervised anomaly detection. In *International Conference on Learning Representations*, 2020. URL <https://openreview.net/forum?id=HkgHOTEYwH>.

Bernhard Schölkopf, John Platt, John Shawe-Taylor, Alex Smola, and Robert Williamson. Estimating the support of a high-dimensional distribution. In *Advances in Neural Information Processing Systems (NeurIPS)*, 2001.

Mei-Ling Shyu, Shu-Ching Chen, Kun Sarinnapakorn, and Li Chang. A novel anomaly detection scheme based on principal component classifier. Technical report, University of Miami, 2003.

Jian Tang, Zhixiang Chen, Ada Wai-Chee Fu, and David W. Cheung. Enhancing effectiveness of outlier detections for low density patterns. In *Pacific-Asia Conference on Knowledge Discovery and Data Mining (PAKDD)*, pages 535–548, 2002.

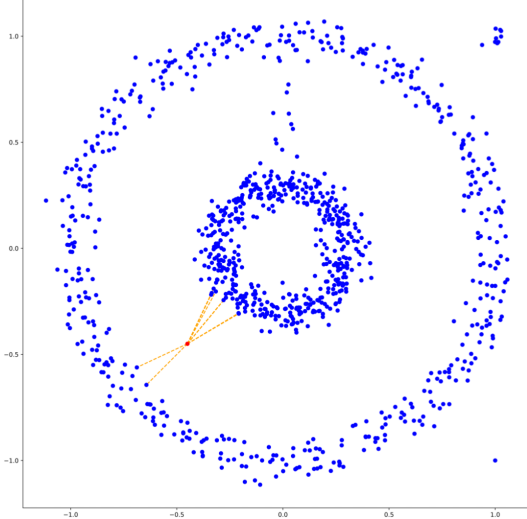
Jaemin Yoo, Lingxiao Zhao, and Leman Akoglu. Self-tuning self-supervised image anomaly detection, 2025. URL <https://arxiv.org/abs/2306.12033>.

Yue Zhao and Maciej K Hryniwicki. Xgbod: improving supervised outlier detection with unsupervised representation learning. In *2018 International Joint Conference on Neural Networks (IJCNN)*, pages 1–8. IEEE, 2018.

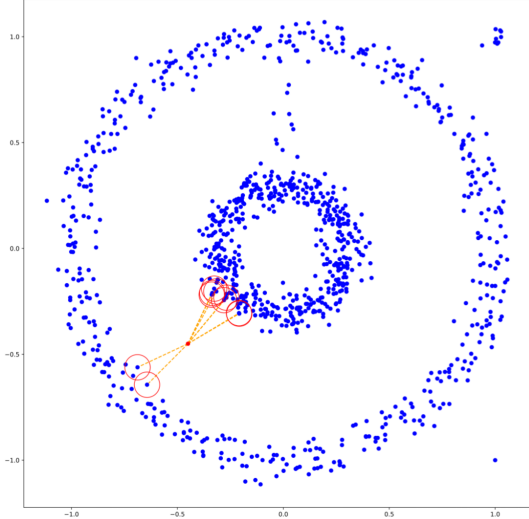
Yingjie Zhou, Xucheng Song, Yanru Zhang, Fanxing Liu, Ce Zhu, and Lingqiao Liu. Feature encoding with autoencoders for weakly supervised anomaly detection. *IEEE Transactions on Neural Networks and Learning Systems*, 33(6):2454–2465, June 2022. ISSN 2162-2388. doi: 10.1109/TNNLS.2021.3086137. URL <http://dx.doi.org/10.1109/TNNLS.2021.3086137>.

Bo Zong, Qi Song, Martin Min, Wei Cheng, Cristian Lumezanu, Daeki Cho, and Haifeng Chen. Deep autoencoding gaussian mixture model for unsupervised anomaly detection. In *International Conference on Learning Representations (ICLR)*, 2018.

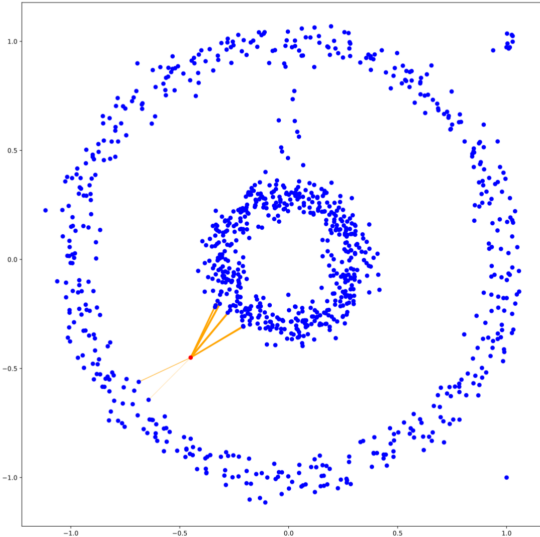
## A Additional detailed results



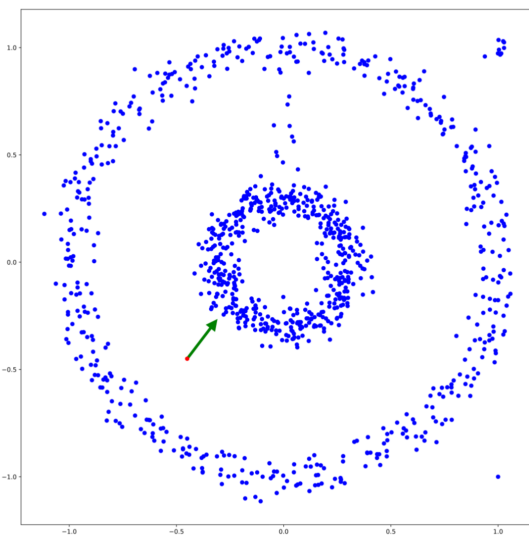
(a) **Initial data representation.** Input samples embedded in the original feature space prior to manifold-aware processing.



(b) **Manifold similarity construction.** A fuzzy neighborhood graph captures local geometric relationships among samples.



(c) **Weighted mean-shift evolution.** Samples are iteratively shifted toward dense manifold regions using empirical neighborhood weights.



(d) **Anomaly scoring via cumulative displacement.** Points exhibiting larger total movement are assigned higher anomaly scores.

Figure 3: **Step-by-step illustration of the proposed MSDE algorithm.** The method constructs a manifold-aware similarity structure, performs weighted mean-shift updates, and quantifies anomaly likelihood using cumulative point displacement.

## A.1 Algorithm Overview

Figure 3 illustrates the key stages of the proposed MSDE framework. The algorithm begins by representing the input data in its original feature space (Fig. 3a). A manifold-aware similarity graph is then constructed using fuzzy neighborhood relationships, capturing local geometric structure (Fig. 3b).

Next, an iterative weighted mean-shift procedure is applied, where each point is updated based on the empirical density of its neighborhood on the learned manifold (Fig. 3c). This process causes samples in dense regions to stabilize quickly, while isolated samples undergo larger displacements.

Finally, the cumulative displacement across iterations is used as an anomaly score (Fig. 3d), with larger movements indicating higher anomaly likelihood.

Table 6: Performance comparison of anomaly detection methods under varying noise levels.

Method	Noise	AUC-ROC $\uparrow$	AUC-PR $\uparrow$	Precision@n $\uparrow$
MSDE	0.00	<b>0.921</b>	<b>0.713</b>	<b>0.694</b>
CBLOF		0.903	0.688	0.667
COF		0.815	0.568	0.545
COPOD		0.855	0.624	0.588
DAGMM		0.822	0.516	0.499
ECOD		0.852	0.624	0.584
HBOS		0.853	0.631	0.600
IForest		0.908	0.666	0.638
KNN		0.910	0.676	0.654
LODA		0.847	0.612	0.583
LOF		0.794	0.574	0.555
OCSVM		0.856	0.650	0.621
PCA		0.865	0.641	0.616
SOD		0.877	0.637	0.617
MSDE	0.01	<b>0.921</b>	<b>0.713</b>	<b>0.694</b>
CBLOF		0.903	0.687	0.666
COF		0.814	0.567	0.544
COPOD		0.855	0.623	0.588
DAGMM		0.822	0.517	0.501
ECOD		0.852	0.624	0.584
HBOS		0.853	0.631	0.599
IForest		0.908	0.666	0.638
KNN		0.910	0.677	0.655
LODA		0.847	0.612	0.583
LOF		0.794	0.574	0.555
OCSVM		0.856	0.649	0.621
PCA		0.865	0.641	0.616
SOD		0.867	0.636	0.616

*Continued on next page*

Method	Noise	AUC-ROC ↑	AUC-PR ↑	Precision@n ↑
MSDE	0.05	<b>0.920</b>	<b>0.710</b>	<b>0.690</b>
CBLOF		0.900	0.676	0.653
COF		0.819	0.569	0.545
COPOD		0.853	0.621	0.586
DAGMM		0.811	0.498	0.482
ECOD		0.851	0.623	0.583
HBOS		0.852	0.630	0.598
IForest		0.906	0.663	0.635
KNN		0.913	0.690	0.664
LODA		0.846	0.610	0.581
LOF		0.801	0.574	0.556
OCSVM		0.852	0.645	0.616
PCA		0.864	0.641	0.610
SOD		0.877	0.636	0.614
MSDE	0.10	0.916	<b>0.705</b>	<b>0.686</b>
CBLOF		0.893	0.661	0.642
COF		0.820	0.552	0.527
COPOD		0.852	0.621	0.588
DAGMM		0.780	0.455	0.445
ECOD		0.850	0.623	0.583
HBOS		0.852	0.631	0.600
IForest		0.904	0.659	0.630
KNN		<b>0.919</b>	0.702	0.678
LODA		0.841	0.600	0.570
LOF		0.806	0.577	0.557
OCSVM		0.841	0.635	0.607
PCA		0.863	0.640	0.614
SOD		0.870	0.621	0.599
MSDE	0.25	0.894	0.680	0.657
CBLOF		0.875	0.658	0.634
COF		0.804	0.505	0.481
COPOD		0.847	0.614	0.578
DAGMM		0.705	0.349	0.347
ECOD		0.846	0.618	0.579
HBOS		0.853	0.636	0.605
IForest		0.893	0.652	0.623
KNN		<b>0.912</b>	<b>0.704</b>	<b>0.678</b>
LODA		0.834	0.586	0.555
LOF		0.808	0.561	0.541
OCSVM		0.819	0.608	0.575
PCA		0.861	0.642	0.615
SOD		0.851	0.601	0.579

*Continued on next page*

Method	Noise	AUC-ROC ↑	AUC-PR ↑	Precision@n ↑
MSDE		0.852	0.619	0.593
CBLOF		0.853	0.636	0.611
COF		0.770	0.462	0.439
COPOD		0.837	0.597	0.560
DAGMM		0.638	0.247	0.252
ECOD		0.837	0.596	0.557
HBOS	0.50	0.854	0.630	0.598
IForest		<b>0.871</b>	0.617	0.588
KNN		<b>0.871</b>	<b>0.652</b>	<b>0.625</b>
LODA		0.800	0.514	0.486
LOF		0.783	0.524	0.502
OCSVM		0.795	0.557	0.524
PCA		0.855	0.632	0.606
SOD		0.852	0.601	0.579

Table 7: Performance comparison of anomaly detection methods under varying synthetic modes.

Method	Synthetic Modes	AUC-ROC ↑	AUC-PR ↑	Precision@n ↑
MSDE		0.834	0.390	0.389
MSDE (opt)		0.880	0.521	0.515
CBLOF		0.837	0.376	0.368
COF		0.886	<b>0.569</b>	0.553
COPOD		0.608	0.149	0.107
DAGMM		0.652	0.211	0.225
ECOD	Dependency	0.597	0.147	0.098
HBOS		0.600	0.147	0.109
IForest		0.782	0.251	0.235
KNN		<b>0.895</b>	0.567	<b>0.556</b>
LODA		0.649	0.172	0.154
LOF		0.879	<b>0.569</b>	<b>0.556</b>
OCSVM		0.624	0.163	0.128
PCA		0.626	0.169	0.135
SOD		0.893	0.542	0.532
MSDE	Cluster	0.952	0.886	0.861
MSDE (opt)		0.944	0.868	0.841
CBLOF		0.889	0.828	0.802
COF		0.521	0.271	0.254
COPOD		0.969	0.927	0.900
DAGMM		0.931	0.732	0.704
ECOD		0.947	0.855	0.819
HBOS		0.970	0.928	0.909
IForest		0.969	0.918	0.886
KNN		0.835	0.503	0.475

*Continued on next page*

Method	Synthetic Modes	AUC-ROC $\uparrow$	AUC-PR $\uparrow$	Precision@n $\uparrow$
LODA		0.917	0.827	0.793
LOF		0.447	0.229	0.218
OCSVM		0.956	<b>0.941</b>	0.919
PCA		<b>0.979</b>	0.936	<b>0.929</b>
SOD		0.758	0.474	0.457
MSDE		0.998	0.958	0.935
MSDE (opt)		0.998	0.958	0.937
CBLOF		0.997	0.952	0.924
COF		0.945	0.824	0.788
COPOD		0.991	0.904	0.865
DAGMM		0.913	0.688	0.649
ECOD	Global	0.990	0.910	0.871
HBOS		0.993	0.922	0.887
IForest		0.997	0.943	0.913
KNN		<b>0.999</b>	<b>0.975</b>	<b>0.960</b>
LODA		0.979	0.904	0.862
LOF		0.916	0.788	0.758
OCSVM		0.987	0.925	0.894
PCA		0.993	0.930	0.899
SOD		0.989	0.953	0.922
MSDE		0.904	0.620	0.593
MSDE (opt)	Local	0.912	0.635	0.608
CBLOF		0.891	0.599	0.575
COF		0.907	0.609	0.585
COPOD		0.853	0.516	0.482
DAGMM		0.791	0.433	0.419
ECOD		0.875	0.587	0.552
HBOS		0.850	0.529	0.497
IForest		0.885	0.556	0.520
KNN		0.912	0.661	0.627
LODA		0.843	0.546	0.523
LOF		<b>0.936</b>	<b>0.710</b>	<b>0.689</b>
OCSVM		0.858	0.571	0.544
PCA		0.864	0.529	0.503
SOD		0.870	0.580	0.558

**Effect of hyperparameter optimization.** In addition to the default MSDE configuration, we report results for **MSDE (opt)**, where hyperparameters are tuned separately for each synthetic mode using Optuna with 10 optimization trials. As shown in Table 7, MSDE (opt) consistently improves performance over the default configuration under *Dependency*, *Global*, and *Local* synthetic modes across all evaluation metrics.

For the *Cluster* mode, MSDE (opt) exhibits slightly lower performance than the default MSDE. We attribute this behavior to the limited optimization budget: with only 10 trials, the hyperparameter search may not sufficiently explore configurations that favor highly separable, globally compact cluster structures. In such settings, the default MSDE parameters designed to emphasize conser-

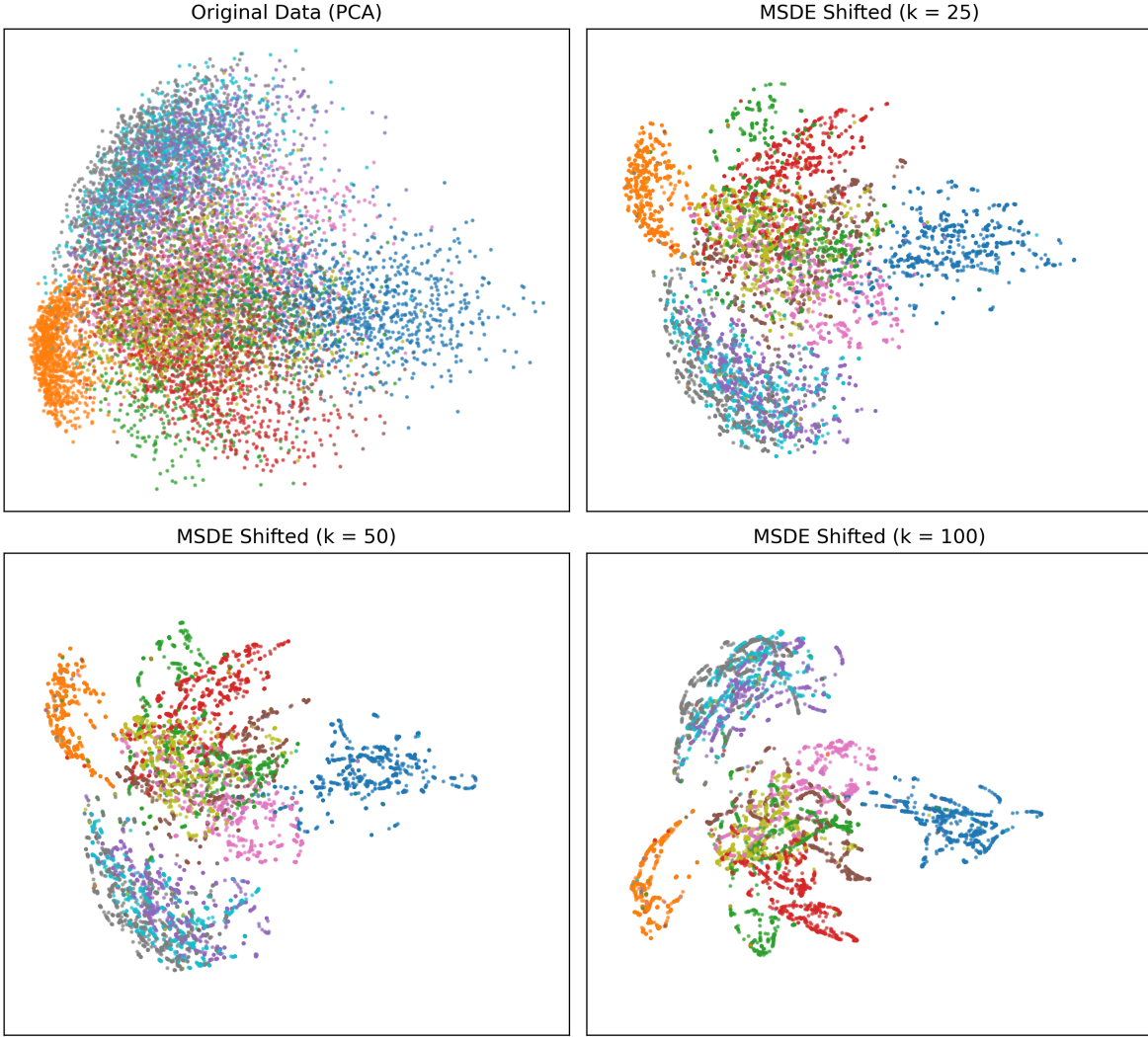


Figure 4: Geometric effect of Mean Shift Density Enhancement (MSDE) visualized in a two-dimensional PCA projection. **Top-left:** original data distribution of MNIST dataset. **Top-right and bottom:** data after MSDE updates (on the MNIST dataset) with increasing neighborhood sizes ( $k = 25, 50, 100$ ) and learning rate of 1. As  $k$  increases, points are progressively attracted toward stable, high-density manifold regions, while samples originating in low-density or unstable regions undergo larger, more directed displacements. This illustrates the central principle of MSDE: anomalous points exhibit greater geometric instability under density-driven manifold evolution.

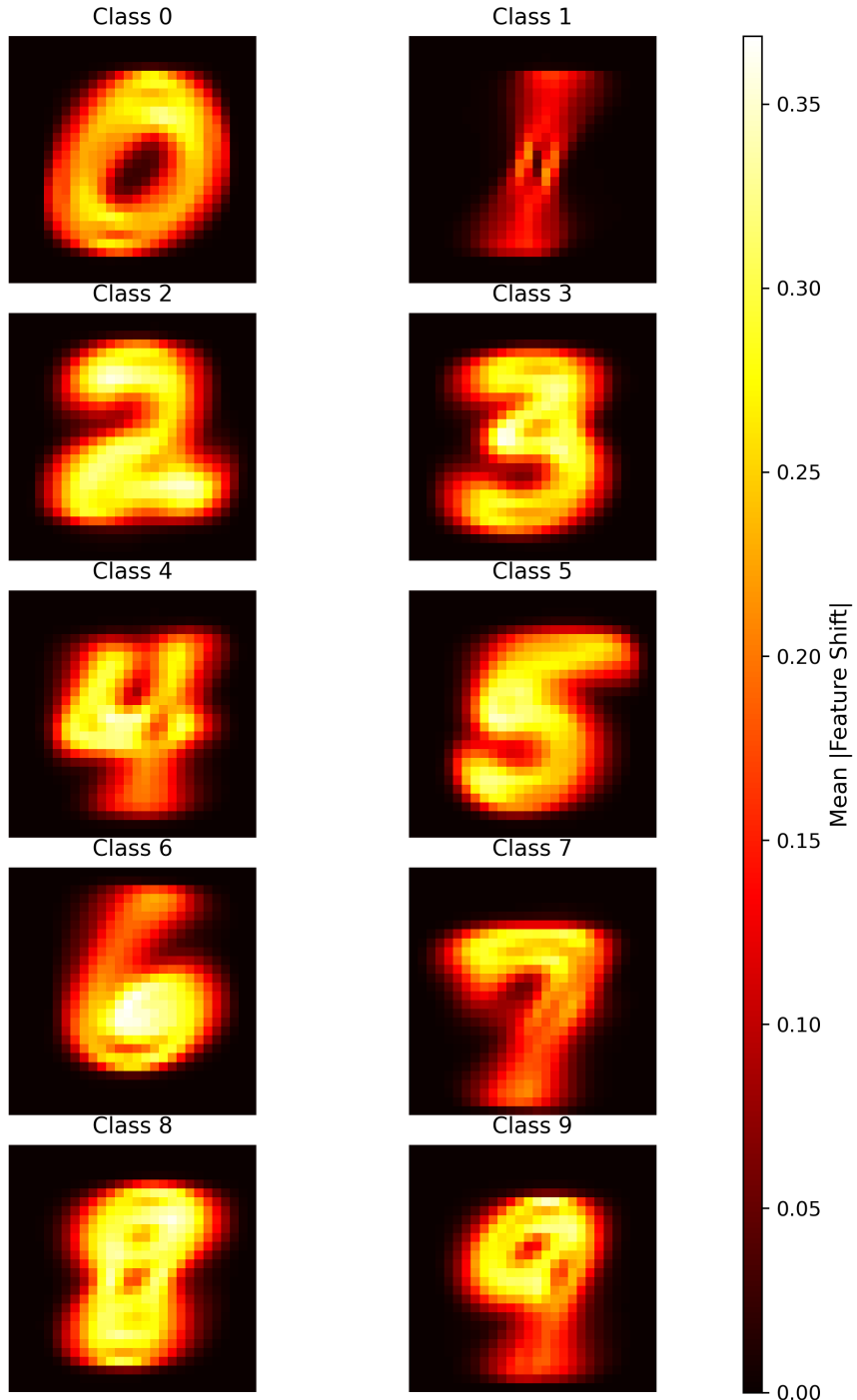


Figure 5: Class-wise visualization of mean absolute feature displacement induced by MSDE on the MNIST dataset. For each digit class, pixel intensities represent the average magnitude of per-feature shift accumulated during the mean-shift iterations. Displacement is concentrated along digit strokes and structurally informative regions, while background pixels remain largely stable. This indicates that MSDE-driven density enhancement selectively perturbs semantically meaningful features rather than introducing diffuse or global distortion.

vative neighborhood aggregation already align well with the underlying data geometry. Increasing the number of optimization trials or adopting mode-specific search spaces is expected to close this gap.

Overall, these results demonstrate that MSDE is robust to hyperparameter choices, while targeted optimization can further enhance performance in most anomaly regimes.

Table 8: Optimized MSDE hyperparameters obtained via Optuna for each synthetic anomaly mode.

Synthetic Mode	$k$	$T_{\text{nbd}}$	$\eta$	$T$	$\tau$	$\theta$
Dependency	13	35	0.0945	19	$2.25 \times 10^{-4}$	0.294
Cluster	82	67	0.1171	7	$2.69 \times 10^{-4}$	0.138
Global	61	70	0.1210	20	$1.19 \times 10^{-4}$	0.115
Local	26	32	0.1303	13	$2.98 \times 10^{-5}$	0.045

## B Scalability Experiments

### B.1 Dataset Description

We performed a small-scale scalability analysis of the proposed **Mean Shift Density Enhancement (MSDE)** method on the Credit Card Fraud Detection dataset [Le Borgne et al., 2022] released by ULB. The dataset contains **284,807 real-world credit card transactions**, among which only **492 are fraudulent** (approximately **0.17%**), making it extremely imbalanced. All features are numerical and anonymized through PCA transformation, except for the transaction amount and timestamp. Due to its large sample size, severe class imbalance, and frequent adoption in anomaly detection literature, this dataset serves as a challenging and realistic benchmark for scalability analysis.

### B.2 Experimental Setup

All experiments were conducted using the *ADBench* framework to ensure a standardized evaluation protocol across methods. MSDE was compared against a diverse set of unsupervised anomaly detection models, including density-based, distance-based, ensemble-based, and probabilistic approaches.

We report the **average total runtime**, which includes both model fitting and inference time. To enable fair comparison across models with substantially different computational characteristics, runtimes are reported on a **logarithmic scale**.

### B.3 Runtime Scalability Analysis

Figure 6 presents the average total runtime of all evaluated models on the Credit Card Fraud dataset.

MSDE demonstrates **moderate computational cost**, outperforming several computationally intensive models such as KNN, DAGMM, SOD, and OCSVM, while remaining more expensive than lightweight linear or histogram-based methods (e.g., PCA and HBOS). The **COF** model failed to complete execution due to excessive memory consumption. As a result, runtime and performance metrics for COF are not reported. Distance-based neighborhood methods exhibit a sharp increase in runtime, highlighting their limited scalability on large datasets.

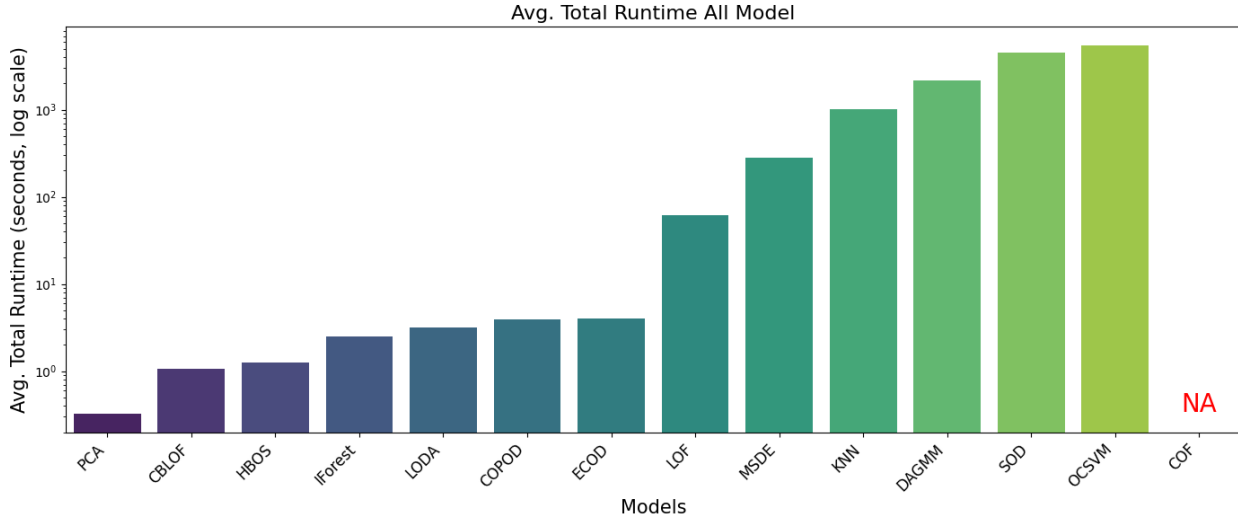


Figure 6: Average total runtime (log scale) of anomaly detection models on the Credit Card Fraud dataset. COF failed due to excessive memory requirements and is therefore excluded.

Table 9: Performance comparison on the Credit Card Fraud dataset.

Model	AUC-ROC	AUC-PR	Precision@N
MSDE	<b>0.964</b>	0.289	0.354
PCA	0.959	0.173	0.250
ECOD	0.958	0.250	0.331
HBOS	0.958	0.253	0.340
COPOD	0.956	0.281	0.354
IForest	0.955	0.160	0.232
CBLOF	0.952	<b>0.435</b>	0.475
KNN	0.949	0.150	0.207
OCSVM	0.923	0.390	0.471
SOD	0.918	0.048	0.119
DAGMM	0.898	0.431	<b>0.502</b>
LODA	0.860	0.262	0.367
LOF	0.511	0.002	0.007
COF	NA	NA	NA

#### B.4 Detection Performance Comparison

Table 9 summarizes the mean detection performance of all models in terms of AUC-ROC, AUC-PR, and Precision@N, which collectively capture ranking quality and detection effectiveness under severe class imbalance.

#### B.5 Discussion

MSDE achieves the **highest AUC-ROC** among all evaluated methods, indicating superior overall ranking capability, while maintaining competitive AUC-PR and Precision@N compared to strong precision-oriented baselines such as DAGMM and CBLOF.

Importantly, MSDE offers a **favorable trade-off between detection performance and computational scalability**, making it well-suited for large-scale, real-world fraud detection scenarios. The failure of COF further emphasizes the necessity of memory-efficient algorithmic design when handling datasets with hundreds of thousands of samples.